Journal of Power Sources 236 (2013) 250–258

Contents lists available at SciVerse ScienceDirect

Journal of Power Sources

journal homepage: www.elsevier.com/locate/jpowsour

Different oxygen redox participation for bulk and surface: A possible global explanation for the cycling mechanism of $Li_{1.20}Mn_{0.54}Co_{0.13}Ni_{0.13}O_2$

Hideyuki Koga [a,b], Laurence Croguennec [a,*], Michel Ménétrier [a], Philippe Mannessiez [a], François Weill [a], Claude Delmas [a]

[a] CNRS, Université de Bordeaux, ICMCB – 87 Avenue Schweitzer, Pessac F-33608, France
[b] Toyota Motor Europe NV/SA, Hoge Wei 33, B-1930 Zaventem, Belgium

HIGHLIGHTS

- A Li and Mn-rich layered oxide with controlled structure and particle size.
- During the 1st charge, irreversible structural reorganization and phase separation.
- Particles' size and cycling conditions affect the distribution between the *two phases*.
- Oxygen participates in the redox processes as oxygen oxidation (bulk) and oxygen loss (surface).

ARTICLE INFO

Article history:
Received 11 October 2012
Received in revised form
23 February 2013
Accepted 25 February 2013
Available online 6 March 2013

Keywords:
Layered oxide
Lithium batteries
X-ray diffraction
Overcapacity
Oxygen oxidation
Oxygen loss

ABSTRACT

Synthesis of $Li_{1.20}Mn_{0.54}Co_{0.13}Ni_{0.13}O_2$ at different temperatures allows modifying particle sizes and specific surface areas while keeping very similar structures for the materials from the local scale to long distances. X-ray diffraction analysis reveals that irreversible structural reorganization of this lithium and manganese-rich layered oxide occurs during the 1st charge and continues during a few cycles. A mixture of *two phases* is formed on the high voltage *plateau* and is then maintained, showing that the material obtained upon cycling is metastable and out of equilibrium. Depending on the particles' size and on the cycling conditions (Cycling rate, temperature and number of cycles) the nature of the materials formed changes, with especially a difference in distribution between the *two phases* observed. We propose that these phenomena are intimately linked to oxygen participation to the redox processes, for one phase with (reversible) oxygen oxidation only and for the second phase up to (irreversible) oxygen loss.

1. Introduction

Lithium-ion batteries have been used already for quite a while to power portable devices such as cellular phones and notebooks, but they are now expected to store and deliver enough energy and power to answer the requirements for transportation and especially those for hybrid and electric vehicles. The most commonly used lithium-ion batteries remain those with the layered oxide $LiCoO_2$ and the carbon graphite at the positive and negative electrodes, respectively. Due to the high cost and possibly low resource of Co, a very intense research effort is currently under progress in order to propose alternatives to $LiCoO_2$ at the positive electrodes [1]. $LiNi_{1-y-z}Co_yAl_zO_2$ is currently used in batteries developed for hybrid electric vehicles and for military and space applications. $LiFe^{II}PO_4$, made of cheap and abundant constituents and with a redox voltage around 3.45 V *vs.* Li^+/Li, is presently the most praised electrode material for the next generation of Li-ion batteries to power electric vehicles as it remains chemically and thermally highly stable over the entire potential window [2,3]. Nevertheless, its weakness remains its low energy density compared to the layered oxide materials. More recently prospective research was performed on other polyanionic materials such as silicates [2], diphosphates [4], borates [5], fluorophosphates [6–9] and fluorosulphates [10–13], in order in all cases to try to gain in energy density.

In parallel to the research on polyanionic materials, the Lithium-rich layered oxides belonging to the $(1-x)LiMO_2 \cdot xLi_2MnO_3$ system

* Corresponding author. Tel.: +33 (0) 5 4000 2234, +33 (0) 5 4000 2647; fax: +33 (0) 5 4000 2761.
E-mail address: crog@icmcb-bordeaux.cnrs.fr (L. Croguennec).

0378-7753/$ – see front matter © 2013 Elsevier B.V. All rights reserved.
http://dx.doi.org/10.1016/j.jpowsour.2013.02.075

(M = Ni, Co) are considered as very attractive materials as they deliver larger capacity with lower cost than $LiCoO_2$ [14–16]. These overlithiated materials (Li/M > 1) revealed a long *plateau* observed only during the first charge of the battery, which is uncommon in classical layered oxides $Li_{1-x}M_{1+x}O_2$ ($x \geq 0$ and M = Ni, Co mainly) [17]. This unusual mechanism is expected to be at the origin of the large capacity observed for these overlithiated materials. The mechanisms involved during the charge–discharge of this type of materials have been addressed recently [17–21] but deeper structural characterizations are still required in order to understand the structure of the materials formed upon cycling and the origin of these very attractive capacities. This paper focuses on $Li_{1.20}Mn_{0.54}Co_{0.13}Ni_{0.13}O_2$ also possibly written as 0.4 $LiNi_{1/3}Mn_{1/3}Co_{1/3}O_2$–0.4 Li_2MnO_3 with high capacity. The composition and structure of different $Li_{1.20}Mn_{0.54}Co_{0.13}Ni_{0.13}O_2$ materials, obtained by the sol–gel method followed by a thermal treatment at 800 °C, 900 °C or 1000 °C, were analysed in detail. As we reported in a previous paper [22], they are very similar whatever the synthesis temperature, with a cation ordering in the transition metal layers and a quasi-ideal layered structure. We also showed that these materials are clearly not made of separate domains of Li_2MnO_3 and $LiNi_{1/3}Mn_{1/3}Co_{1/3}O_2$, but that they are solid solutions with ordered domains limited to a few layers along the *c*-axis. In the present paper, we report on the structural changes observed using X-ray diffraction for $Li_{1.20}Mn_{0.54}Co_{0.13}Ni_{0.13}O_2$ upon cycling, depending on the particle size of the active material and on the cycling conditions (number of cycles, cycling rate and temperature).

2. Experimental

Three materials of composition $Li_{1.20}Mn_{0.54}Co_{0.13}Ni_{0.13}O_2$ were prepared at temperatures of 800 °C, 900 °C or 1000 °C using the sol–gel method, as described in detail in Ref. [22]. They were characterized by X-ray diffraction (XRD) using a Siemens D5000 diffractometer equipped with a detector using energy discrimination and Cu Kα radiation, in the 10–80° ($2\theta_{Cu}$) range, with steps of 0.02° ($2\theta_{Cu}$) and a constant counting time of 15 s. The profile matching and Rietveld refinement of the XRD patterns were performed using the Fullprof software [23]. The morphology of the powders was observed by scanning electron microscopy (SEM) using a Hitachi S4500 field emission microscope with an accelerating voltage of 5.0 kV. The materials were coated with a thin layer of platinum in order to prevent any charge accumulation on their surface. Surface area measurements were carried out by the Brunauer, Emmet and Teller (B.E.T) method with a Quantachrome Autosorb-1 device after the sample was dried overnight under vacuum at 300 °C.

The electrochemical properties of the prepared materials were tested using CR2325 coin cells with lithium metal as negative electrode. The positive electrodes consisted of 80 wt% of active material, 10 wt% of a carbon black/graphite (1:1) mixture and 10 wt % of polyvinylidene difluoride (PVdF) binder and were cast from a *N*-methylpyrrolidone (NMP) based slurry on an aluminium foil. They were then pressed at 40 MPa after drying at 80 °C during overnight. The cells were assembled in an argon filled glove box with the electrolyte 1 M $LiPF_6$ dissolved in a mixture of propylene carbonate (PC), ethylene carbonate (EC), and dimethylcarbonate (DMC) 1:1:3 by volume. The electrochemical measurements were performed between 2.5 and 4.8 V *vs.* Li^+/Li, the cycling rate being defined so that 1 C rate corresponds to a theoretical exchange of one electron in 1 h. *Ex situ* X-ray diffraction was performed on lithium deintercalated materials recovered from batteries at different states of charge and discharge. Before their analysis they were washed with DMC in large excess, dried at room temperature under vacuum and prepared in a specific sample-holder to prevent any contact with ambient atmosphere and thus avoid their evolution.

3. Results and discussion

3.1. Composition, structure and microstructure of the powders prepared at different temperatures

As detailed in Refs. [22], the XRD patterns obtained for the three $Li_{1.20}Mn_{0.54}Co_{0.13}Ni_{0.13}O_2$ materials prepared at 800 °C, 900 °C or 1000 °C are compared in Fig. 1a. All the main peaks, except for the extra broad and small intensity peaks observed between 20 and 30° ($2\theta_{Cu}$) (enlarged in Fig. 1b) can be indexed based on a hexagonal cell described in the space group *R-3m* (α-$NaFeO_2$-type structure). The cell parameters $a_{hex.}$ and $c_{hex.}$ were determined to be ~2.851 Å and ~14.235 Å, respectively. As expected, the crystallinity of the powders increases with temperature, as shown by the sharpening of the X-ray diffraction lines from 0.19° to 0.12° for $FWHM_{(003)}$ and from 0.29° to 0.19° for $FWHM_{(104)}$ when the synthesis temperature increases from 800 °C to 1000 °C. The extra lines observed in the [20–30°] angular range can be indexed considering a $\sqrt{3}.a_{hex.} \times \sqrt{3}.a_{hex.}$ superstructure in the transition metal planes and reveal the presence of an ordering between the large (Li^+, Ni^{II}) cations on one site and the small (Mn^{IV}, Co^{III}) cations on the other site, by analogy to the Li_2MnO_3 structure (described in the *C2/m* space group). As shown by the width and relative intensity of these extra lines, and as supported by electron diffraction data [22], the ordering in the transition metal layers is rather extended whereas the correlation between the ordered slabs is restricted along the *c*-axis. Despite a significant difference in their crystallinity, these three materials were shown to be very similar in structure, with *(i)* a quasi ideal 2D structure (the Li^+/Ni^{II} exchange between the

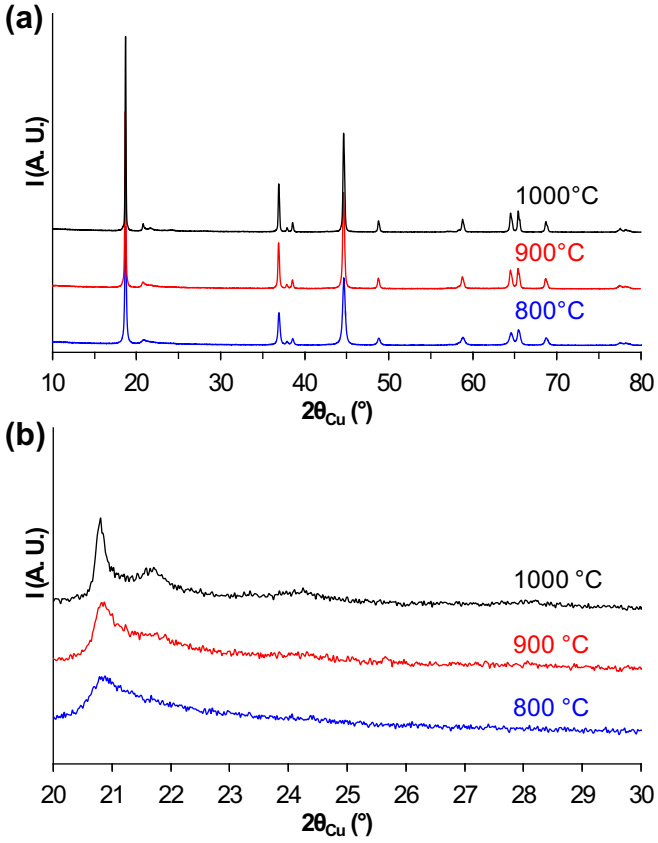

Fig. 1. (a) X-ray diffraction patterns of $Li_{1.20}Mn_{0.54}Co_{0.13}Ni_{0.13}O_2$ synthesized at 800 °C, 900 °C and 1000 °C in the 10–80° ($2\theta_{Cu}$) range. (b) Detailed XRD data in the 20–30° angular range.

slab and the interslab space is indeed limited to less than 0.02) and *(ii)* a very similar local ordering of cations as revealed by ^{7}Li MAS NMR, Raman and electron diffraction data [22].

Fig. 2 gives a comparison of the SEM micrographs obtained for the three materials. The primary particle size increases with the heating temperature from 50 nm to 500 nm in diameter. The higher the synthesis temperature, the sharper are the edges of the primary particles, suggesting a better crystallization. The specific surface area of these powders decreases with an increase of the thermal-treatment temperature and is equal to 9.9 $m^2\ g^{-1}$, 4.3 $m^2\ g^{-1}$ and 3.6 $m^2\ g^{-1}$ for the compounds obtained at 800 °C, 900 °C and 1000 °C, respectively.

3.2. Structural changes observed during the first cycle

The 1st cycle curves obtained for the lithium cells prepared with the three compounds as positive electrode materials and cycled at the C/20 rate in the 2.5–4.8 V *vs.* Li^+/Li potential window are compared in Fig. 3. The three curves are very similar, as expected from the very similar composition and structure of the powders. Upon charge the potential evolves, in a first step, continuously with lithium composition, then a voltage *plateau* is observed around 4.5 V *vs.* Li^+/Li and, finally, a continuous evolution of the potential is again observed during the discharge over the whole lithium composition range. Large irreversible capacities are observed at the first cycle (more than 15% of the first charge capacity), with a first discharge capacity around 270 mAh g^{-1} (Fig. 3). This reversible capacity is around 230 mAh g^{-1} during the first 10 cycles [22] and decreases gradually down to 200 mAh g^{-1} at the 100th cycle. The effect of the synthesis temperature of $Li_{1.20}Mn_{0.54}Co_{0.13}Ni_{0.13}O_2$ is not obvious on the cycling performance since the differences observed here remain of the order of the reproducibility of the experiments.

XRD analysis was carried out *ex situ* for $Li_{1.20}Mn_{0.54}Co_{0.13}Ni_{0.13}O_2$ prepared at 1000 °C for different lithium compositions during the first charge and the following discharge of the battery. Eight XRD patterns are compared in Fig. 4, for key lithium compositions: 1.20 (pristine material), 0.88 (beginning of the *plateau*), 0.63, 0.37 (during the *plateau*) and 0.12 (end of the *plateau*) and then, 0.43, 0.69 and 0.98 at different discharge states. These results reveal first a fast broadening of the diffraction lines upon lithium deintercalation, as especially highlighted for the *(003)* line in Fig. 4b by

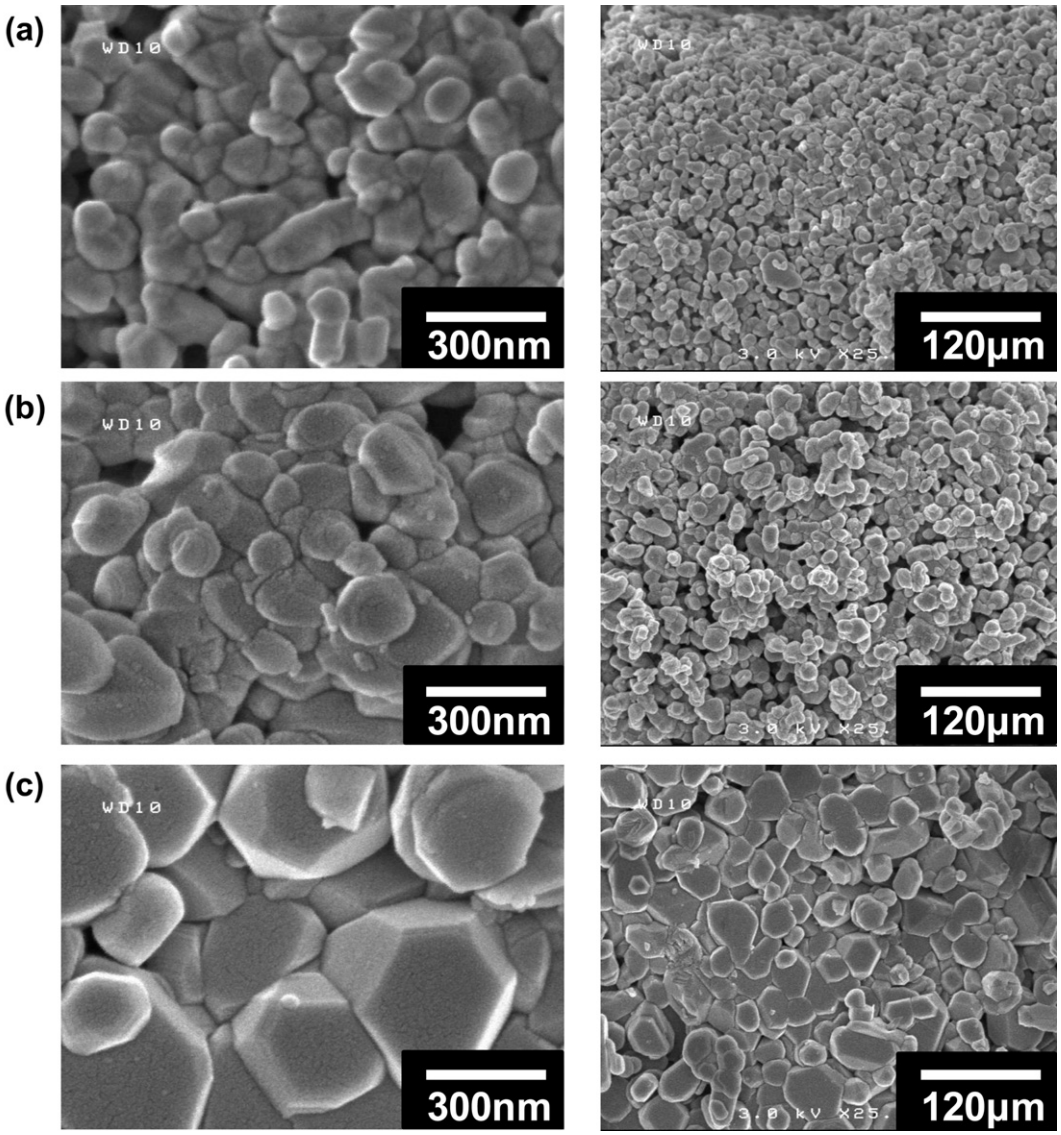

Fig. 2. SEM images of $Li_{1.20}Mn_{0.54}Co_{0.13}Ni_{0.13}O_2$ synthesized at (a) 800 °C, (b) 900 °C and (c) 1000 °C.

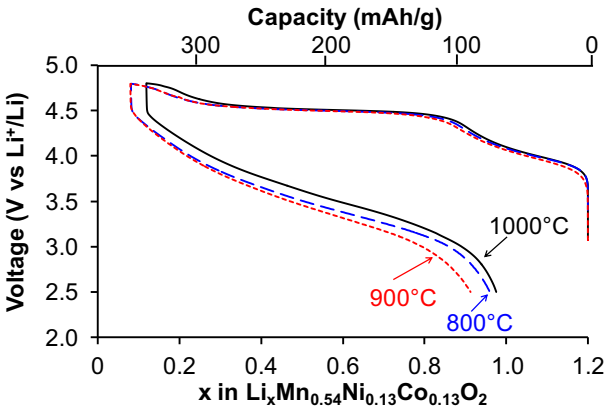

Fig. 3. The 1st cycle curves obtained at a rate of C/20 for different Li//$Li_xMn_{0.54}Co_{0.13}Ni_{0.13}O_2$ cells, $Li_{1.20}Mn_{0.54}Co_{0.13}Ni_{0.13}O_2$ being synthesized at 800 °C, 900 °C and 1000 °C.

the enlargement of the [18–19.5° ($2\theta_{Cu}$)] angular range. Then, from the beginning of the *plateau* two sets of diffraction lines that can be fully indexed in the *R-3m* space group are observed; they are maintained – with changes in the cell parameters – all along the *plateau* in charge and during the next discharge. At the end of the first discharge, as especially shown in Fig. 4d with the observation of the *(104)* line, two sets of diffraction lines are still present. In addition, the enlargement given in the [20–30° ($2\theta_{Cu}$)] angular range in Fig. 4c reveals the irreversible broadening and decrease in intensity of the extra lines associated to the superstructure due to the cation ordering in the slabs.

Changes in the lattice parameters with lithium composition (*x* in $Li_xMn_{0.54}Co_{0.13}Ni_{0.13}O_2$) are given in Fig. 5 (in blue in web version upon charge and in red upon discharge) and Table 1. An example of refinement is given in supplementary information in Figure S1 (by the Le Bail method for the material $Li_{1.20}Mn_{0.54}Co_{0.13}Ni_{0.13}O_2$ (1000 °C) recovered after one cycle at C/20 rate at room temperature). From the beginning of the *plateau* in the first charge, all the XRD patterns were analysed considering the presence of two lamellar oxide phases. The $a_{hex.}$ cell parameter decreases at the beginning of the first charge and maintains around 2.834 Å for the two phases formed during the *plateau*. During the discharge the $a_{hex.}$ cell parameter continuously increases in parallel for the two phases (Fig. 5a). As shown in Fig. 5b the $c_{hex.}$ cell parameter increases at the beginning of the first charge and then decreases for the two phases on the *plateau* so that they can be best separated at the end of the charge. During the following discharge the two

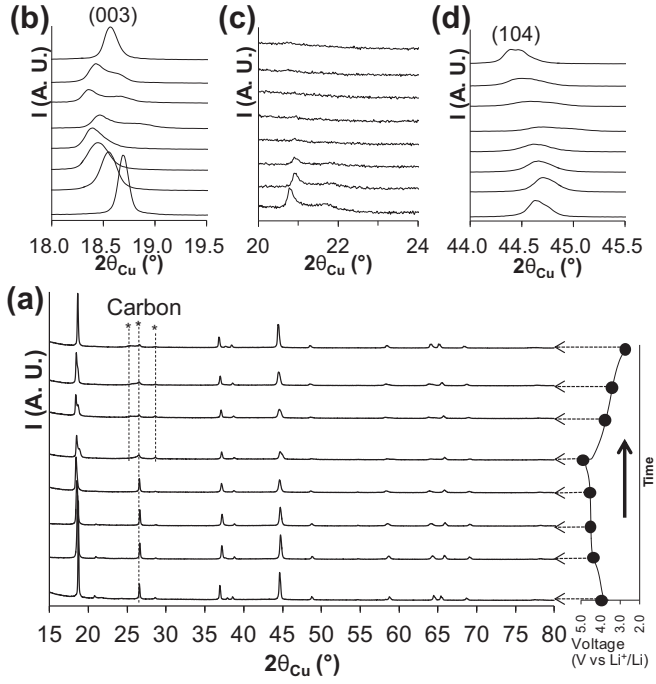

Fig. 4. (a) X-ray diffraction patterns of $Li_{1.20}Mn_{0.54}Co_{0.13}Ni_{0.13}O_2$ recovered during the 1st cycle at different states of charge and discharge of the lithium battery. A typical electrochemical curve is given on the right part of the figure in order to indicate the lithium composition of the material studied. (b) Detailed XRD data in the 18–19.5° ($2\theta_{Cu}$) angular range, (c) in the 20–22° ($2\theta_{Cu}$) angular range, and (d) in the 44–45.5° ($2\theta_{Cu}$) angular range.

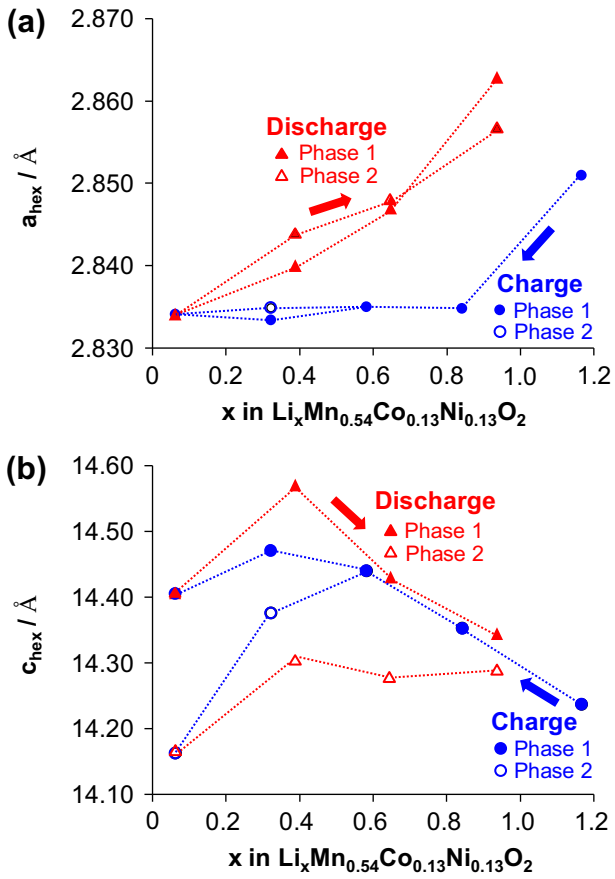

Fig. 5. Changes in lattice parameters, $a_{hex.}$ (a) and $c_{hex.}$ (b), *vs.* lithium composition (*x* in $Li_xMn_{0.54}Co_{0.13}Ni_{0.13}O_2$) during the 1st charge and discharge. Due to the presence of these two phases in the material formed upon cycling, *x* defines the average composition in lithium for the mixture but not that of each phase.

Table 1
Changes in lattice parameters during the 1st charge and discharge.

	x ($Li_xMn_{0.54}Co_{0.13}Ni_{0.13}O_2$)	Phase 1		Phase 2	
		$a_{hex.}$	$c_{hex.}$	$a_{hex.}$	$c_{hex.}$
Charge	1.16	2.851(2)	14.237(3)	–	–
	0.84	2.8348(2)	14.353(3)	–	–
	0.58	2.835(2)	14.44(2)	–	–
	0.32	2.8334(3)	14.472(2)	2.8349(4)	14.376(4)
	0.07	2.8341(3)	14.406(3)	2.8342(2)	14.163(1)
Discharge	0.39	2.84(2)	14.57(2)	2.844(2)	14.31(1)
	0.65	2.847(2)	14.43(2)	2.848(1)	14.28(1)
	0.94	2.8629(2)	14.344(2)	2.8568(7)	14.29(3)

phases remain, their $c_{hex.}$ cell parameters first increase and then decrease upon lithium intercalation. The value of $a_{hex.}$ is highly correlated to the average oxidation state of the transition metal ions since it corresponds to the metal–metal distance in the MO_2 slab. A decrease of $a_{hex.}$ is thus associated to a decrease of the transition metal ionic radius and therefore to its oxidation and, conversely, an increase associated to its reduction. The absence of change in $a_{hex.}$ suggests no change in the oxidation state of the transition metal ions on the *plateau* despite lithium deintercalation [19], whereas the continuous increase of the $a_{hex.}$ cell parameter during the discharge suggests (contrary to what is observed during the preceding charge) a continuous reduction of the transition metal ions. $c_{hex.}$ first expands upon lithium deintercalation due to increasing electrostatic repulsions between the oxygen layers forming the interslab space since the deintercalated lithium ions do not play their screening role anymore. Upon further lithium deintercalation the Metal–Oxygen bond becomes more and more covalent leading to less charged oxygen ions and thus to a shrinkage of $c_{hex.}$ Even if the global evolution of $c_{hex.}$ is expected for classical $Li_{1-x}M_{1+x}O_2$ layered oxides ($x \geq 0$) [24], the uncommon evolution of $a_{hex.}$ as a function of the lithium content in $Li_xMn_{0.54}Co_{0.13}Ni_{0.13}O_2$ and the formation of two phases after the *plateau* highlight the occurrence of a complex lithium deintercalation mechanism in this overlithiated manganese-rich layered oxide during the first charge.

Biphased domains are often observed for classical layered oxides at the end of the 1st charge when total removal of Li ions from the structure requires for instance stabilization of another oxygen packing: an O1-type structure (with an *AB* oxygen packing as in CdI_2) is for instance formed for NiO_2 through a two-phase domain involving NiO_2 and $Li_{1/4}NiO_2$ [24]. In the case of $Li_{1.20}Mn_{0.54}Co_{0.13}Ni_{0.13}O_2$, the phase observed at the beginning of the *plateau* transforms into a mixture of two new phases, without any change in the oxygen packing, instead of progressively disappearing to the benefit of a new phase. Furthermore, the two phases formed evolve in parallel on the *plateau* with further lithium deintercalation. We have observed as shown in Fig. 4 that a global broadening of the lines occurs during the first charge and is maintained during the next discharge, suggesting an increasing disorder in the material with a decrease of the coherent domains size. From X-ray diffraction experiments only, we cannot describe in depth the organization of these domains formed upon cycling. The XRD patterns were calculated taking into account the presence of *two phases*, but in fact each of them is most probably an average description of a distribution of phases with very close composition and cation distributions. It is also essential to mention that the appearance of this two-phase mixture cannot be associated to a heterogeneity that would be already present in the pristine material, indeed combining diffraction (X-rays, neutrons and electrons), NMR and Raman spectroscopies the homogeneity of $Li_{1.20}Mn_{0.54}Co_{0.13}Ni_{0.13}O_2$ was confirmed from longer to more local scales [22]. Finally, the $c_{hex.}/a_{hex.}$ ratio determined for the phases formed upon cycling remains always larger than 5 and is thus significantly different from 4.90 which is expected for a long range spinel-type structure. Nevertheless, it does not prevent the formation at the local scale of domains with transition metal ions in the interslab spaces, usually improperly called spinel phase in literature.

3.3. Effect of the powder particle size and cycling conditions on the phase separation

Similar analyses were performed for the $Li_{1.20}Mn_{0.54}Co_{0.13}Ni_{0.13}O_2$ material synthesized at 800 °C and 900 °C, and the results are compared to those obtained for the sample synthesized at 1000 °C in Fig. 6. We chose here to restrict the XRD patterns to the

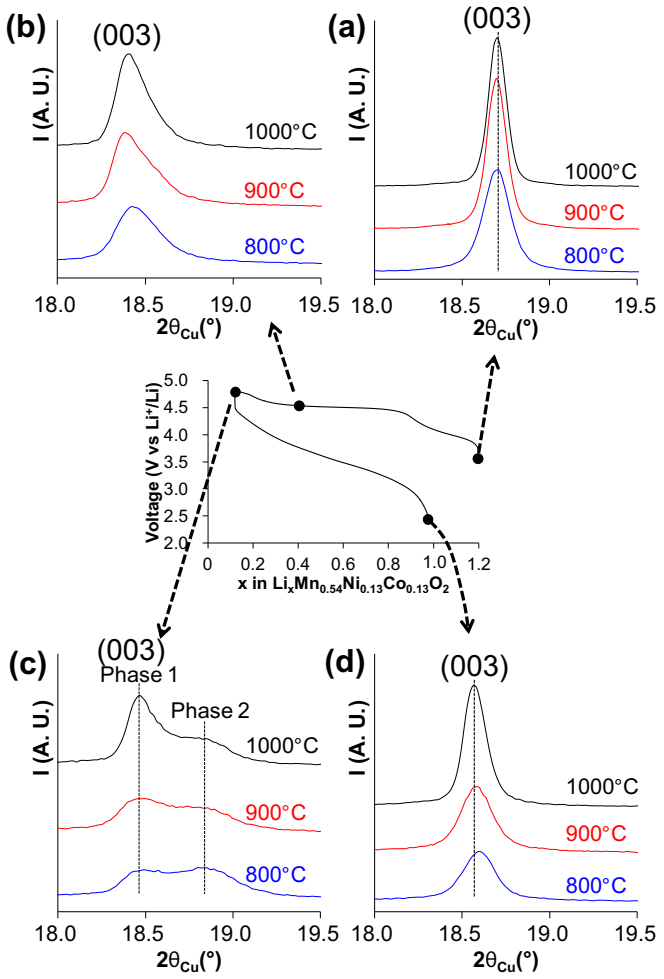

Fig. 6. Changes in the X-ray diffraction patterns of $Li_xMn_{0.54}Co_{0.13}Ni_{0.13}O_2$ synthesized at 800 °C, 900 °C and 1000 °C and recovered from the batteries at different states of charge and discharge during the 1st cycle: (a) in the initial state, (b) on the *plateau*, (c) at the end of the *plateau* and (d) at the end of the 1st cycle. The angular range is limited to 18–19.5° ($2\theta_{Cu}$) in order to focus especially on the *(003)* diffraction lines.

(003) lines angular range in order to highlight changes in the phase diagram. Whatever the synthesis temperature of $Li_{1.20}Mn_{0.54}Co_{0.13}Ni_{0.13}O_2$, phase separation occurs from the beginning of the *plateau*; furthermore the amount of phase 2 (smaller $c_{hex.}$) *vs.* phase 1 (larger $c_{hex.}$) increases when the particle size decreases and thus when the specific surface area increases.

Fig. 7a shows the cycling curves obtained for lithium cells with $Li_{1.20}Mn_{0.54}Co_{0.13}Ni_{0.13}O_2$ synthesized at 1000 °C as positive electrode material: the 1st, 2nd, 10th, 50th and 100th charges and discharges obtained at C/20 rate and at room temperature are compared. The reversible discharge capacity was shown to reach ~200 mAh g^{-1} at the 100th cycle. The shape of the charge and discharge curves evolves continuously during the first fifty cycles, as even more clearly highlighted by the differential curves $dQ/dV = f(V)$ given in Fig. 7b. Then almost no changes are observed during the next fifty cycles. During the first cycles all the redox processes involved during lithium deintercalation and reintercalation occur above 3.2 V *vs.* Li^+/Li, with (after the 1st charge) two main potential ranges in charge and in discharge as pointed out by the two dotted lines *A* and *B*. Upon further cycling the redox processes involved partially shift to lower voltages as shown by line *C* (down to 2.75 V *vs.* Li^+/Li in discharge), with the disappearance of the intermediate potential process (line *B*) and maintenance of the

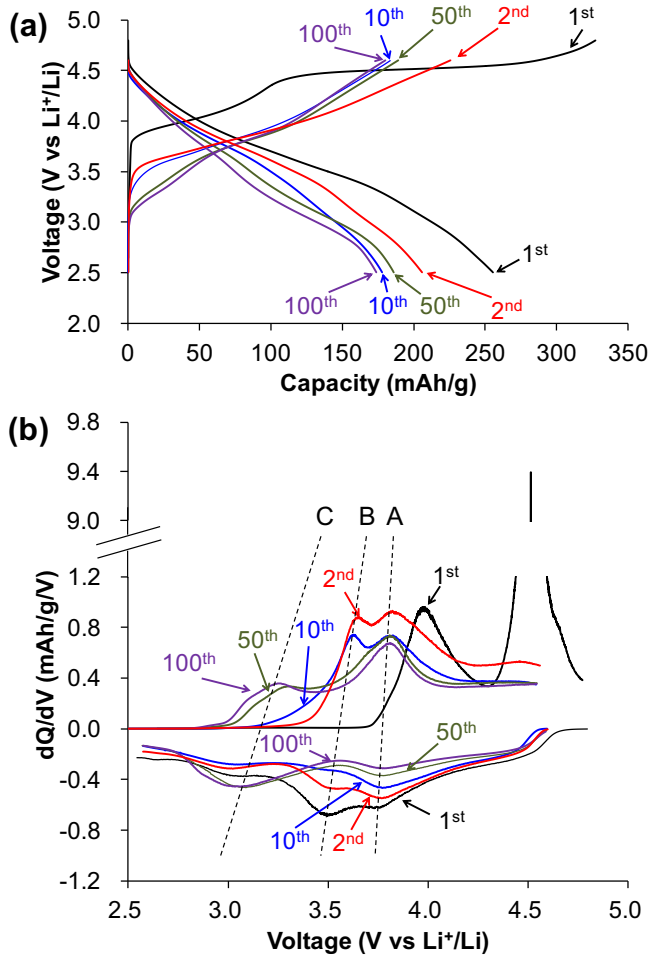

Fig. 7. (a) Comparison of the 1st, 2nd, 10th, 50th and 100th charge–discharge curves obtained for Li//$Li_{1.20}Mn_{0.54}Co_{0.13}Ni_{0.13}O_2$ cells with $Li_{1.20}Mn_{0.54}Co_{0.13}Ni_{0.13}O_2$ prepared at 1000 °C. (b) Corresponding differential curves $dQ/dV = f(V)$.

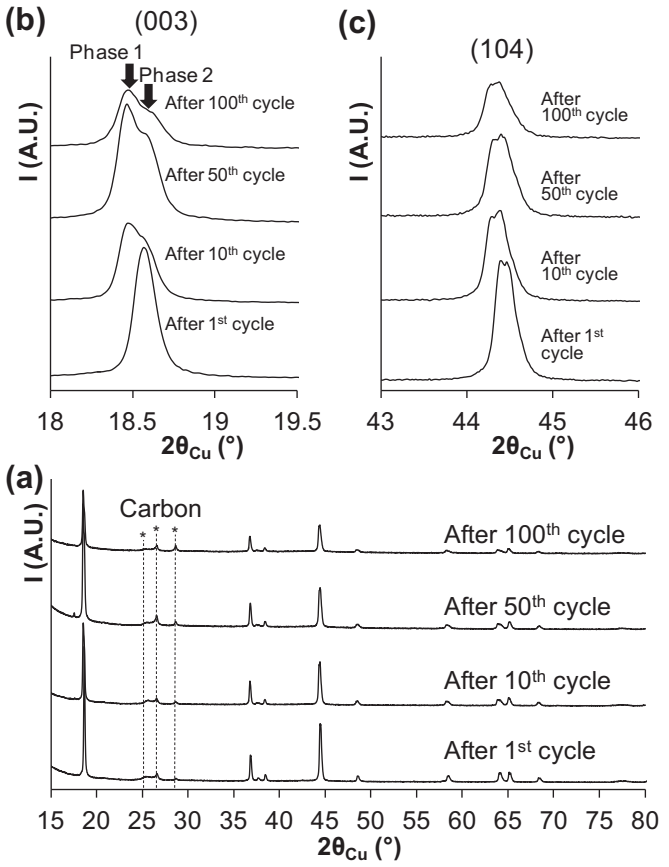

Fig. 8. X-ray diffraction patterns of $Li_{1.20}Mn_{0.54}Co_{0.13}Ni_{0.13}O_2$ synthesized at 1000 °C and recovered from the batteries after the 1st, 10th, 50th and 100th cycle (a); detailed XRD data in the 18–19.5° ($2\theta_{Cu}$) range (b) and in the 43–46° ($2\theta_{Cu}$) range (c).

higher potential one (line *A*). These results suggest a continuous structural modification of the material during the first fifty cycles, with in addition a change in the redox couples involved in the lithium (de)intercalation reactions: manganese ions might therefore participate to the redox processes. Indeed, it is interesting to recall that for *layered* O3-$LiMn^{III}O_2$ (monoclinic [25,26]), lithium deintercalation from the *layered* structure occurs during the 1st charge at 3.6–3.7 V *vs.* Li^+/Li with the oxidation of Mn^{3+} to Mn^{4+}. Then, upon cycling *layered* Li_xMnO_2 material transforms into spinel type structure with redox processes in two potential ranges, one around 3.0 V and another around 4.0 V *vs.* Li^+/Li. In the case of $Li_{1.20}Mn_{0.54}Co_{0.13}Ni_{0.13}O_2$ the redox process *B* (that disappears) could thus be associated to the Mn^{4+}/Mn^{3+} redox couple in the layered stacking, and the redox process *C* observed after tens of cycles could be associated to the Mn^{4+}/Mn^{3+} redox couple in the domains with transition metal ions in the interslab spaces. As shown in Fig. 8 (and especially in Fig. 8c), whatever the number of cycles the material recovered at the end of the discharge is a mixture of *two phases*. With an increasing number of cycles the heterogeneity of the material increases as revealed by the larger broadening of the X-ray diffraction lines. Furthermore, the amount of *phase 2* (smaller $c_{hex.}$) increases *vs.* that of *phase 1* (larger $c_{hex.}$) upon cycling. However despite the number of cycles no formation of long range spinel-type structure is observed: the ratio $c_{hex.}/a_{hex.}$ remains around 5.

The impact of a smaller charge rate (C/100; *i.e.* in conditions closer to the equilibrium) and of higher cycling temperature (55 °C) on the homogeneity of the material formed upon cycling was checked *vs.* classical conditions (charge at C/20 rate and at 25 °C). The corresponding cycling curves are given in Fig. 9 and the X-ray diffraction data recorded at the end of these first cycles in Fig. 10. Although almost no difference is observed between the three charges (except a slight decrease in potential for lower rate and higher temperature), an obvious difference in shape and in reversible capacity exists between the three discharges. The XRD patterns reveal the formation of still heterogeneous samples, with an increasing amount of *phase 2* (smaller $c_{hex.}$) *vs. phase 1* (larger $c_{hex.}$).

Altogether it appears that whatever the cycling conditions (cycling rate, number of cycles, cycling temperature) and powder particle size, the materials formed upon cycling from the beginning of the *plateau* are and remain heterogeneous. This shows that, whatever the conditions, the materials are far from equilibrium.

3.4. Discussion

According to the composition of the samples and to the oxidation states of the transition metal cations ($Li_{1.20}Mn^{IV}_{0.54}Co^{III}_{0.13}Ni^{II}_{0.13}O_2$) in the pristine materials, the first part of the charge is expected to be associated to the oxidation of Ni and Co to the tetravalent state (up to $Li0.81Mn^{IV}0.54Co^{IV}0.13Ni^{IV}0.13O_2$), and the *plateau* to a deintercalation of Li that was proposed by Lu et al. to be compensated for by oxygen loss [17]. As already reported, oxygen evolution is a

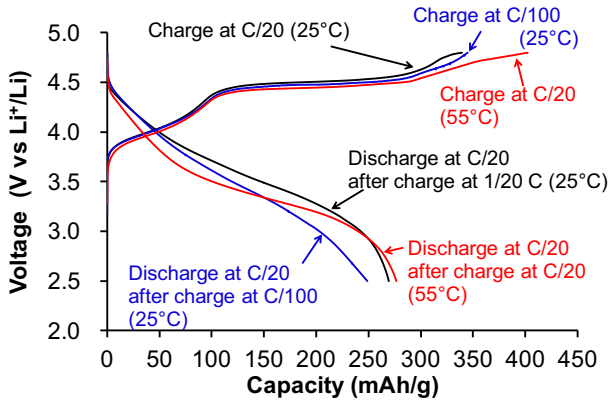

Fig. 9. Comparison of the first charge and discharge curves obtained for Li// $Li_{1.20}Mn_{0.54}Co_{0.13}Ni_{0.13}O_2$ cells in different conditions of cycling: charge with cycling rates of C/20 or C/100, discharge with cycling rate of C/20, cycling temperature of 25 °C or 55 °C.

unique property of these Li excess manganese-rich materials but the mechanism involved is still not clear. As we already discussed in Ref. [19] for $Li_{1+x}(Ni_{0.425}Mn_{0.425}Co_{0.15})_{1-x}O_2$, two models can theoretically be considered to account for the oxygen evolution, even if only the second is expected from solid state chemist's considerations:

- 1st model: oxygen is lost at the surface and oxygen ions diffuse within the bulk (from inside to outside); oxygen vacancies are thus formed and distributed within the material. Considering this model (Reaction I), lithium vacancies would remain in the slabs and could be theoretically filled by lithium ions during the next discharge with the involvement of the Mn^{4+}/Mn^{3+} redox couple.

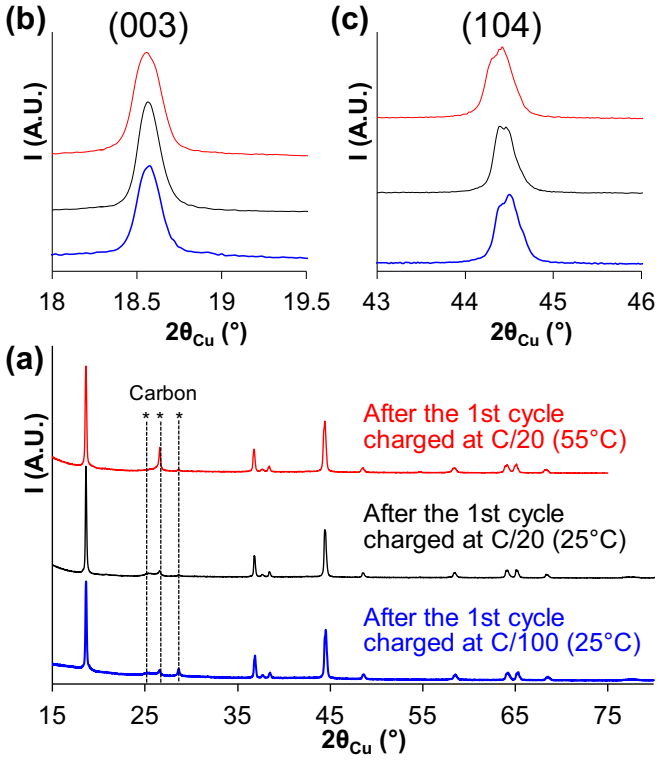

Fig. 10. Comparison of the X-ray diffraction patterns obtained for the material $Li_{1.20}Mn_{0.54}Co_{0.13}Ni_{0.13}O_2$ recovered from lithium cells charged in different conditions. All the discharges were performed at a C/20 rate.

$$\text{Reaction I}: \left(Li_{0.98}Ni^{II}_{0.02}\right)\left(Li_{0.22}Mn^{IV}_{0.54}Ni^{II}_{0.11}Co^{III}_{0.13}\right) O_2 \rightarrow \left(\square_{\mathbf{0.98}}Ni^{III}_{0.02}\right)\left(\square_{\mathbf{0.22}}Mn^{IV}_{0.54}Ni^{IV}_{0.11}Co^{IV}_{0.13}\right) (\mathbf{O_{1.58}}\square_{\mathbf{0.42}}) + 1.20Li^+ + 1.20e^- + 0.21O_2 \quad (1)$$

This formula is proposed for the fully deintercalated composition considering lithium deintercalation with the formation of oxygen vacancies and, as already shown for $Li_{1-z}Ni_{1+z}O_2$ [27], that the nickel ions present in the interslab spaces are oxidized up to the trivalent state only.

- 2nd model: oxygen loss occurs at the surface with migration of the transition metal ions from the surface to the bulk. Indeed, due to the oxygen loss the transition metal ions present at the surface are expected to be unstable as MO_5 environments and would thus migrate from the surface to the bulk in the sites left vacant by the lithium ions already deintercalated in the slabs. This mechanism (Reaction II) would induce a shrinkage of the host structure, but also a decrease in the number of Li sites that can be occupied during the following discharge (0.78 *vs.* 1.20 initially).

$$\text{Reaction II}: \left(Li_{0.98}Ni^{II}_{0.02}\right)\left(Li_{0.22}Mn^{IV}_{0.54}Ni^{II}_{0.11}Co^{III}_{0.13}\right)O_2 \rightarrow \mathbf{0.79}\left(\left(\square_{\mathbf{0.975}}Ni^{III}_{0.025}\right)\left(\square_{\mathbf{0.02}}Mn^{IV}_{0.68}Ni^{IV}_{0.14}Co^{IV}_{0.16}\right)(\mathbf{O_2}) + 1.20Li^+ + 1.20e^- + 0.21O_2 \quad (2)$$

This formula proposed for the fully deintercalated composition is obtained considering, in comparison to that proposed for the first model, a full densification of the oxygen lattice (here O_2 *vs.* $O_{1.58}\square_{0.42}$ with more than 20% of oxygen vacancies for the former) and thus a shrinkage of the host structure (here 0.79 mol of MO_2 *vs.* 1 mol of $M_{0.80}(O_{1.58}\square_{0.42})$ for the former).

In good agreement with our previous conclusions for $Li_{1+x}(Ni_{0.425}Mn_{0.425}Co_{0.15})_{1-x}O_2$ [19], we can conclude that the 1st model cannot explain the mechanism involved in our $Li_{1.20}Mn_{0.54}Co_{0.13}Ni_{0.13}O_2$ compound. Indeed, according to Reaction I, ~1/6 oxygen ions are estimated to be lost from the structure of $Li_{1.20}Mn_{0.54}Co_{0.13}Ni_{0.13}O_2$ after a first full charge based on the Faradays and redox processes of the transition metal ions. Almost all MO_6 environments would thus be changed to MO_5, and it is known that Mn^{4+} and Ni^{4+} ions are not stable into MO_5 environments.

Therefore, considering the 2nd model, densification occurs inducing a decrease in the number of possible Li sites per transition metal ion. In that case, the discharge capacity (with participation of manganese in addition to nickel and cobalt to the redox processes) could be estimated to ~230 mAh g^{-1} after the 1st cycle (*i.e.* exchange of maximum 0.78 Li^+ ions) whereas it is in fact larger than 270 mAh g^{-1} (*i.e.* more than 0.90 Li^+ ions exchanged). The 2nd model involving densification, only by itself, can thus not account for the total number of electrons exchanged during the first discharge even if it remains the most realistic from solid state chemists' considerations.

The large capacity obtained could be explained from a theoretical point of view by a combination between the two models but as already mentioned the main cations present in the material in the charge state (Mn^{4+} and Ni^{4+}) are not stable in MO_5 environments which restricts the extent of the first mechanism which therefore cannot account for the experimentally obtained capacity. This discrepancy between the experimental and the expected reversible discharge capacities thus strongly suggests that oxygen participation to the redox processes, without oxygen loss but with oxygen oxidation, has to be considered as proposed by Koyama, Goodenough and Ito in particular [21,28,29]. The pinning of the

manganese t_{2g} band at the top of the oxygen *p* band makes that latter available for oxidation and charge compensation for Lithium deintercalation. This assumption is also supported by XAS results obtained by different authors [20,21,30]: manganese participation to the redox processes occurs, as suggested also by our experimental electrochemical data given in Fig. 7, but is not sufficient to explain the number of electrons exchanged in the first discharge.

Our XRD analysis has shown the formation of *two phases* upon cycling, with larger amount of *phase 2* for smaller particles and for cycling conditions closer to equilibrium. At the present stage, considering only XRD data, it is of course difficult to describe the microstructure of these materials but we can reasonably make the hypothesis that *phase 2* would be formed preferentially at the particles' surface and *phase 1* remains in the bulk. As the densification mechanism involves transition metal diffusion in the solid and oxygen loss at the surface, *phase 2* would then most probably be the densified phase obtained after loss of the oxidized oxygen ions formed at the surface during the first charge [19]. Only the transition metal ions would participate to the redox processes involved during further cycling of *Phase 2* ($Ni^{4+}/Ni^{3+}/Ni^{2+}$, Co^{4+}/Co^{3+} and Mn^{4+}/Mn^{3+}). *Phase 1* would be rather similar in structure to the pristine material, with also the involvement of three redox couples, but in that case two cationic redox couples only ($Ni^{4+}/Ni^{3+}/Ni^{2+}$ and Co^{4+}/Co^{3+}) and one anionic redox couple ($O^{2-\delta}/O^{2-}$).

Our experimental results combined with those reported by other authors in literature [20,21,30,31] lead us to propose this mechanism: **oxygen loss at the surface** with densification of the host structure and reversible **oxygen oxidation within the bulk** without oxygen loss and without major modification of the structure. Experiments are currently in progress in order to characterize these materials recovered after cycling, which are clearly heterogeneous and *composites*, and to check these hypotheses: aberration corrected scanning transmission electron microscopy and nano beam electron diffraction experiments to get more insights into the local structure of these materials (distribution between the *two phases* and evolution upon cycling), but also *in situ* XAS to follow changes in the redox processes upon cycling.

From the results discussed in the present paper, it appears that the *plateau* observed in the first charge is correlated to the "extra" capacity obtained during the subsequent cycling of lithium and manganese-rich layered oxides. In our model, this *plateau* is due to the surface reaction of the material with oxygen oxidation and loss, which induces a reconstruction (densification) of the outer part of the crystallites. However, a reversible oxygen oxidation also occurs in the bulk of the material during this first charge, but this is not detected on the voltage since the contact with the electrolyte is via the surface where this densification reaction occurs. Once this irreversible reaction has been completed on the first charge, the *plateau* is no longer observed during the following charges and the voltage traduces the complex (reversible) combined redox reactions of the transition metals and of oxygen. These surface reaction and reconstruction appear necessary but not sufficient to activate the reversible oxygen oxidation/reduction reaction in lithium-rich layered oxide materials. Indeed, our group previously observed densification only for $Li_{1+x}(Ni_{0.425}Mn_{0.425}Co_{0.15})_{1-x}O_2$ ($x \leq 0.12$) [19], whereas we report here combination of densification at the surface with reversible oxygen oxidation/reduction in the bulk for $Li_{1.20}Mn_{0.54}Co_{0.13}Ni_{0.13}O_2$. Changes in the electronic structure during the first charge is essential, with as discussed by Koyama and Goodenough a huge impact of manganese (and thus of the manganese content in the material formula) [28,29].

This mechanism could also explain the effect of a coating on the extent of "oxygen vacancy elimination" as discussed by the group of Manthiram by the comparison of $Li_{1.20}Mn_{0.54}Co_{0.13}Ni_{0.13}O_2$ either coated with a homogeneous layer of Al_2O_3 or bare [32]. Less "oxygen vacancy elimination" or in other words less densification was reported for the Al_2O_3 coated compound. The formation of a coating indeed decreases the *free* specific surface area of the active material (*i.e.* that in contact with the electrolyte); it might thus allow to increase the fraction of oxygen ions stabilized in their oxidized state and thus lead to a decrease of the amount of oxygen ions lost from the structure. It is however important to mention that, even with this coating, the *plateau* observed in the first charge occurs, and the irreversible reaction due to oxygen elimination is decreased, but not suppressed, in agreement with our assumption that this is required to activate the reversible oxygen oxidation/reduction in the bulk of the material.

4. Conclusions

X-ray diffraction analyses reveal that irreversible structural reorganization occurs upon cycling of the lithium and manganese-rich layered oxide $Li_{1.20}Mn_{0.54}Co_{0.13}Ni_{0.13}O_2$ in lithium cells. A mixture of *two phases* is formed on the high voltage *plateau* and is then preserved upon long range cycling, showing that the reactions involved are out of equilibrium. The impact of the particles' size and cycling conditions (Cycling rate, temperature and number of cycles) on the distribution between the *two phases* shows that the surface and the bulk react differently. As it was already proposed, oxygen participates to the reactions involved upon cycling of $Li_{1.20}Mn_{0.54}Co_{0.13}Ni_{0.13}O_2$. This occurs for one phase, rather present in the bulk, through (reversible) oxygen oxidation and, for the other phase, rather present at the surface, through oxidation of oxygen anion with departure of O_2. The origin of these *two phases* would come from the difference in stability for oxidized oxygen ions between the surface and the bulk of the material.

Acknowledgements

The authors would like to thank Cathy Denage (ICMCB) for her technical assistance, Région Aquitaine and Toyota for their financial support.

Appendix A. Supplementary data

Supplementary data related to this article can be found at http://dx.doi.org/10.1016/j.jpowsour.2013.02.075.

References

[1] K. Mizushima, P.C. Jones, P.J. Wiseman, J.B. Goodenough, Mater. Res. Bull. 15 (1980) 783.
[2] B.L. Ellis, K.T. Lee, L.F. Nazar, Chem. Mater. 22 (2010) 691.
[3] M. Maccario, L. Croguennec, F. Le Cras, C. Delmas, J. Power Sources 183 (2008) 411.
[4] S. Nishimura, M. Nakamura, R. Natsui, A. Yamada, J. Am. Chem. Soc. 132 (2010) 13596.
[5] A. Yamada, N. Iwane, Y. Harada, S.-i. Nishimura, Y. Koyama, I. Tanaka, Adv. Mater. 22 (2010) 3583.
[6] N. Marx, L. Croguennec, D. Carlier, A. Wattiaux, F. Le Cras, E. Suard, C. Delmas, Dalton Trans. 39 (21) (2010) 5108.
[7] N. Recham, J.N. Chotard, L. Dupont, C. Delacourt, W. Walker, M. Armand, J.M. Tarascon, Nat. Mater. 9 (2010) 68.
[8] T.N. Ramesh, K.T. Lee, B.L. Ellis, L.F. Nazar, Electrochem. Solid State Lett. 13 (4) (2010) A43.
[9] J.M. Ateba Mba, C. Masquelier, E. Suard, L. Croguennec, Chem. Mater. 24 (2012) 1223.
[10] M.A. Reddy, V. Pralong, V. Caignaert, U.V. Varadaraju, B. Raveau, Electrochem. Commun. 11 (2009) 1807.
[11] P. Barpanda, M. Ati, B.C. Melot, G. Rousse, J.-N. Chotard, M.-L. Doublet, M.T. Sougrati, S.A. Corr, J.-C. Jumas, J.-M. Tarascon, Nat. Mater. 10 (2011) 772.
[12] L. Liu, B. Zhang, X.-J. Huang, Prog. Nat. Sci. Mater. Int. 21 (2011) 211.
[13] R. Tripathi, G. Popov, B.L. Ellis, A. Huq, L.F. Nazar, Energy Environ. Sci. 5 (2012) 6238.
[14] Z. Lu, J.R. Dahn, Electrochem. Solid State Lett. 4 (2001) A191.
[15] Y.J. Park, Y.S. Hong, X. Wu, K.S. Ryu, S.H. Chang, J. Power Sources 129 (2004) 288.

[16] Y. Wu, A. Manthiram, Electrochem. Solid State Lett. 9 (2006) A221.
[17] Z. Lu, L.Y. Beaulieu, R.A. Donaberger, C.L. Thomas, J.R. Dahn, J. Electrochem. Soc. 149 (2002) A778.
[18] A.R. Armstrong, M. Holzapfel, P. Novàk, C.S. Johnson, S.-H. Kang, M.M. Thackeray, P.G. Bruce, J. Am. Chem. Soc. 128 (2006) 8694.
[19] N. Tran, L. Croguennec, M. Ménétrier, F. Weill, Ph. Biensan, C. Jordy, C. Delmas, Chem. Mater. 20 (2008) 4815.
[20] N. Yabuuchi, K. Yoshii, S.T. Myung, I. Nakai, S. Komaba, J. Am. Chem. Soc. 133 (2011) 4404.
[21] A. Ito, Y. Sato, T. Sanada, M. Hatano, H. Horie, Y. Ohsawa, J. Power Sources 196 (2011) 6828.
[22] H. Koga, L. Croguennec, Ph. Mannessiez, M. Ménétrier, F. Weill, L. Bourgeois, M. Duttine, E. Suard, C. Delmas, J. Phys. Chem. C 116 (25) (2012) 13497.
[23] J. Rodriguez-Carvajal, Laboratoire Léon Brillouin (2004). http://www-llb.cea.fr/fullweb/powder.htm.
[24] L. Croguennec, C. Pouillerie, C. Delmas, J. Mater. Chem. 11 (2001) 131.
[25] F. Capitaine, P. Gravereau, C. Delmas, Solid State Ionics 89 (1996) 197.
[26] A.R. Armstrong, P.G. Bruce, Nature 381 (1996) 499.
[27] J.P. Pérès, C. Delmas, A. Rougier, M. Broussely, F. Perton, Ph Biensan, P. Willmann, J. Phys. Chem. Solids 57 (1996) 1057.
[28] Y. Koyama, I. Tanaka, M. Nagao, R. Kanno, J. Power Sources 189 (2009) 798.
[29] J.B. Goodenough, Y. Kim, Chem. Mater. 22 (2010) 587.
[30] Y.S. Hong, Y.J. Park, K.S. Ryu, S.H. Chang, M.G. Kim, J. Mater. Chem. 14 (2004) 1424.
[31] J. Kikkawa, T. Akita, M. Tabuchi, K. Tatsumi, M. Kohyama, J. Electrochem. Soc. 158 (2011) A760.
[32] J. Liu, B. Reeja-Jayan, A. Manthiram, J. Phys. Chem. C 114 (2010) 9528.